SCIENTIFIC REPORTS

Correction: Author Correction

OPEN

Received: 18 April 2017
Accepted: 5 July 2017
Published online: 09 August 2017

Dynamic Mechano-Regulation of Myoblast Cells on Supramolecular Hydrogels Cross-Linked by Reversible Host-Guest Interactions

Marcel Hörning[1,5], Masaki Nakahata[2,6], Philipp Linke[3], Akihisa Yamamoto[1], Mariam Veschgini[3], Stefan Kaufmann[3], Yoshinori Takashima[4], Akira Harada[2] & Motomu Tanaka[1,3]

A new class of supramolecular hydrogels, cross-linked by host-guest interactions between β-cyclodextrin (βCD) and adamantane, were designed for the dynamic regulation of cell-substrate interactions. The initial substrate elasticity can be optimized by selecting the molar fraction of host- and guest monomers for the target cells. Moreover, owing to the reversible nature of host-guest interactions, the magnitude of softening and stiffening of the substrate can be modulated by varying the concentrations of free, competing host molecules (βCD) in solutions. By changing the substrate elasticity at a desired time point, it is possible to switch the micromechanical environments of cells. We demonstrated that the Young's modulus of our "host-guest gels", 4–11 kPa, lies in an optimal range not only for static (*ex situ*) but also for dynamic (*in situ*) regulation of cell morphology and cytoskeletal ordering of myoblasts. Compared to other stimulus-responsive materials that can either change the elasticity only in one direction or rely on less biocompatible stimuli such as UV light and temperature change, our supramolecular hydrogel enables to reversibly apply mechanical cues to various cell types *in vitro* without interfering cell viability.

Ample experimental evidence suggested that biological cells do not only sense and respond to biochemical cues from the surrounding environment but also actively react to the mechanical properties (elasticity) of the extracellular microenvironments[1,2]. There are two signaling pathways regulating such mechano-sensing machineries. First, the clusters of integrin receptors, called focal adhesions, trigger the downstream cascades of intracellular signaling pathways, called "outside-in" signaling. This leads to mechanical force generation via contraction of actin-myosin (actomyosin) complexes[3]. The resistance of the extracellular matrix (ECM) against the traction force determines the connection between integrin clusters and actomyosin complexes, mediated by talin and vinculin. Second, the mechanical stimulation of actomyosin complexes by external cues can also cause the conformational change in the cytoplasmic domains of integrin and strengthen the binding to the extracelluar matrix, called as "inside-out" signaling[4].

To date, various ECM models based on chemically cross-linked hydrogels have been designed[5] to investigate the regulatory principles of mechano-sensing. Through fine adjustment of cross-linker concentrations and the reaction time[6,7], one can control the bulk elasticity (Young's modulus) of a given gel substrate "*ex situ*". Such materials have been used to gain insight into the vital role of elasticity compliance between cells and ECM in optimizing the cell morphology[8–10], regulating the migratory behavior[11,12], and controlling the stem cell differentiation[13,14].

[1]Institute for Integrated Cell-Material Science (WPI iCeMS), Kyoto University, Kyoto, 606-8501, Japan. [2]Project Research Center for Fundamental Sciences, Graduate School of Science, Osaka University, 1-1 Machikaneyama-cho, Toyonaka, Osaka, 560-0043, Japan. [3]Physical Chemistry of Biosystems, University of Heidelberg, D69120, Heidelberg, Germany. [4]Department of Macromolecular Science, Graduate School of Science, Osaka University, 1-1 Machikaneyama-cho, Toyonaka, Osaka, 560-0043, Japan. [5]Present address: Institute of Biomaterials and Biomolecular Systems (IBBS), University of Stuttgart, 70569, Stuttgart, Germany. [6]Present address: Division of Chemical Engineering, Department of Materials Engineering Science, Graduate School of Engineering Science, Osaka University, 1-3 Machikaneyama-cho, Toyonaka, Osaka, 560-8531, Japan. Marcel Hörning and Masaki Nakahata contributed equally to this work. Correspondence and requests for materials should be addressed to A.H. (email: harada@chem.sci.osaka-u.ac.jp) or M.T. (email: tanaka@uni-heidelberg.de)

On the other hand, many *in vivo* studies and experiments using organotypic cultures demonstrated that dynamic changes in the ECM stiffness influence various key functions of cells. For example, transplanted mesenchymal stem cells exhibit a remarkable enhancement of bone regeneration upon the degradation of soft alginate matrix[15]. It was also found that mesenchymal stem cells transplanted near the liver tissue did not adhere or repair the damaged tissue, but settled down in the periportal space[16]. Another medically relevant example is a clear correlation between the ECM density and the migration pattern of cancer cells[17]. These findings inspired the design of a new ECM model, whose mechanical properties can be altered in a time-dependent manner[18].

Recent studies in the field of supramolecular chemistry have shown that reversible bonds formed through specific intermolecular interactions can impart dynamic and adoptive properties to polymer materials[19,20]. To date, a number of polymer materials that respond to external stimuli such as light, redox reaction, pH level, heat, and electric/magnetic fields, have been designed to regulate their mechanical properties[21,22]. However, the external stimuli used in many cases, such as UV light[23] and temperature change[24,25], are cytotoxic and interfere with the cell viability. Several recent studies demonstrated that the thiolated hyaluronic acid[26] and gelatin[27] form chemical gels via disulfide bonds, whose Young's modulus decreased by adding dithiothreitol. However, such materials have a fundamental drawback: the change in the substrate stiffness by the cleavage of disulfide bonds goes only in one direction. Once a bond is cleaved, it can hardly be recovered. Polymers increasing the density of covalent cross-links by external stimuli share the same problem. Once a covalent bond is formed, it is very hard to cleave it.

Previously, we proposed the use of physically cross-linked hydrogels composed of an inter-connected micellar network of triblock copolymer chains possessing pH-responsive blocks at two ends. The elasticity of pH-responsive gels can be modulated by pH titration. The morphological dynamics and adhesion strength of several different cell types could be achieved[28–30]. However, although we observed no major interference with cell viability, a new class of hydrogel substrates that can reversibly alter the elasticity at pH 7.4 is more desirable for broader applications. In this study, we selected cyclodextrin (CD) as a milder chemical stimulus, which is a cyclic oligosaccharide that can act as the "host" for different hydrophobic "guest" molecules. Harada *et al*. have utilized host-guest interactions of CD, and designed a rich variety of hydrogels that are cross-linked with the host-guest interactions[31,32]. Since the association and dissociation of host-guest pairs can readily be achieved by adding either host or guest molecules in solutions, the host-guest polymer materials allow a number of applications[33,34], such as stimuli-responsive actuators[35] and self-healing materials[31,36].

We functionalized the side chain of acrylamide monomers with β-cyclodextrin (βCD), and used them as the host. As the guest moiety, we selected adamantane, which fits well into the hollow cavity inside βCD. By optimizing the mixing ratio between pure acrylamide monomers (matrix) and acrylamide monomers modified with host/guest moieties, we fabricated hydrogels that possess the elastic modulus suited for the culture of myoblasts. This substrate material is advantageous over other commonly used hydrogels: First, the poylacrylamide backbones have widely been utilized for the culture of various cell types. Second, both βCD and adamantane are known to be non-cytotoxic[37,38]. This enabled us to use free cyclodextrin molecules as a molecular stimulus (competitor) that can fine-adjust the chemical equilibrium of cross-links and thus can reversibly alter the substrate elasticity without damaging cells. Details of the experimental findings are summarized in the following sections.

Materials and Methods

Materials. Acrylamide (AAm), $CDCl_3$, and D_2O were purchased from Wako Pure Chemical Industries, Ltd. βCD was obtained from Junsei Chemical Co., Ltd. Triethylamine (Et_3N), sodium hydroxide, hydrochloric acid, ammonium peroxodisulfate (APS), *N*,*N*,*N*′,*N*′–tetramethylethylenediamine (TEMED), and *N*,*N*′–methylenebis(acrylamide) (MBAAm) were purchased from Nacalai Tesque Inc. Acryloyl chloride and vinyltrimethoxysilane were purchased from Tokyo Chemical Industry Co., Ltd. DMSO–d_6 was obtained from Merck & Co., Inc. RPMI-1640 medium, fetal bovine serum, penicillin and streptomycin were purchased from Sigma-Aldrich, Co. LifeAct-TagGFP2 and the Torpedo® lipofection reagent were purchased from ibidi GmbH. A highly porous synthetic resin (DIAION HP–20) used for column chromatography was purchased from Mitsubishi Chemical Co., Ltd. Water used for the preparation of the aqueous solutions was purified with a Millipore Integral MT system. Other reagents were used without further purification.

Sample preparation. Round cover glass ($\varnothing = 25$ mm) were cleaned using a modified RCA method[39]. The substrates were immersed in a 5% (v/v) solution of vinyltrimethoxysilane in toluene and shaken for 18 h at room temperature. After the sequential rinsing in acetone, ethanol, and deionized water, the glass substrates were baked at 140 °C for 1 h in air. The vinyl-silanized glass substrates were protected from UV irradiation until final use.

βCD—Ad gel (*x*,*x*) was prepared according to previous literatures[32,40]. In brief: 6–acrylamido–βCD (βCD—AAm, *x* mol%) and adamantane-acrylamide (Ad—AAm, *x* mol%) were mixed in water at 90 °C in a silicone oil bath for 3–4 h. After cooling, AAm (100–2*x* mol%) was added. Here, *x* represents mol% of βCD–AAm and Ad–AAm monomers. C_m represents the total concentration of βCD—AAm, Ad—AAm, and AAm. After dissolving all monomers, APS and TEMED were added, and a 50 μL portion of the mixed solution was injected in a gap between a vinyl-silanized glass substrate and a hydrophilic, plasma-treated cover glass and kept for 15 min. After removing the cover glass, the sample was successively soaked in excess of DMSO/water (1:1, v/v) for 24 h and in water for 48 h to remove the residual chemicals. The surface of hydrogel substrates was functionalized with fibronectin via bifunctional cross-linker Sulfo-SANPAH (Thermo Scientific), following previous publications (Supporting Information S1)[41,42].

Mechanical properties of host-guest gels. The bulk elasticity of host-guest gels was measured by a Rheoner RE–33005 creep meter (Yamaden Ltd., Tokyo). The elasticity of host-guest gels near the surface was determined by nano-indentation with an atomic force microscope (NanoWizard, JPK Instruments, Berlin). As reported previously, the density of hydrated polymers near the surface is diffusive and thus cannot be treated

like a clear boundary with a Gaussian roughness[43–45]. In order to avoid the artifacts caused by indenting diffusive interface that has a larger length scale than the curvature radius of cantilevers (typically 20–30 nm), we indented the sample with a Pyrex-nitride spherical colloidal probe ($R = 5\,\mu m$) attached to a silicon-nitride cantilever with a nominal spring constant of 0.08 N/m (CP-PNP-BSG; Olympus Optical). The Young's modulus E of the gel was calculated from the nonlinear least-square fitting of the force-indentation curves[46,47]:

$$F = 4ER^{1/2} \cdot [3(1 - \nu)^2]^{-1} \cdot \delta^{3/2} \quad (1)$$

where F is the force applied to the indenter, $\nu = 0.5$ the Poisson's ratio, and δ the indentation depth[48].

Unless stated otherwise, all the data points are from more than three independent measurements, and the error bars in each figure correspond to the standard deviations.

Cell culture. Mouse myoblast cells (C2C12, <20 passages, RIKEN BRC Cell Bank) were cultured in RPMI-1640 medium supplemented with 10 wt% of fetal bovine serum, 100 U/mL penicillin and 100 μg/mL streptomycin. The cells were detached from the culture-flasks by enzymatic digestion using trypsin-EDTA (0.25%, Sigma), and 1×10^4 cells were seeded on the fibronectin-coated substrate 24 h before the observation. The actin filaments in live cells were visualized by transfecting C2C12 with LifeAct-GFP following the manufacturer's protocol (ibidi GmbH). Prior to the experiments, we confirmed that free βCD molecules in solutions have no cytotoxicity by the WST assay (Supporting Information S2).

Morphology analysis. Cell dynamics on hydrogels were monitored by an inverted fluorescence microscope (Zeiss) and a Fast-Scan Confocal Fluorescence Microscope (Nikon, A1R). Morphological parameters, such as projected area A, aspect ratio AR (the ratio between major and minor axes), and circularity

$$C = 4\pi A/(perimeter)^2 \quad (2)$$

Of the adherent C2C12 cells were calculated using algorithms written in Matlab (Mathworks). The nematic order parameter of actin cytoskeletons $<S>$ is calculated from the actin filaments as described before[29,49,50]. The original image was convoluted with the n eLoG kernels and the maximum response image was calculated for each pixel, as

$$I_{max}(x, y) = \max [eLoG(n) \times I(x, y)] \quad (3)$$

I_{max} was processed by an intensity-threshold to obtain the image of the segmented stress fibers[51], and the fibers with the same rotational direction with less than 10 pixels were removed. The order parameter

$$\langle S \rangle = \langle \cos 2\theta \rangle \quad (4)$$

was calculated from the histogram of fiber orientations that were scaled by the corresponding fluorescence intensities to account for the local concentration of actin filaments.

Data availability. All data generated or analyzed during this study are included in this published article (and its Supplementary Information files).

Results and Discussion

Figure 1a shows preparation and chemical structure of the host-guest gel (βCD–Ad gel (x,x)) used as cell culture substrates in this study. The gel was prepared by radical polymerization after dissolving the hydrophobic guest monomers (Ad–AAm) by forming the inclusion complex with the host monomer (βCD–AAm). These monomers were terpolymerized with AAm in aqueous solution, forming a hydrogel. x represents mol% of βCD–AAm and Ad–AAm monomers in the monomer solution. Figure 1b shows how the fraction of βCD–Ad cross-linkages can be modulated by the presence of free βCD molecules in aqueous solution. Free βCD molecules act as competitors and reduce the number of βCD side chains conjugated with Ad. As a consequence, one can fine-adjust the degree of cross-linking and thus the Young's modulus E of gels by adjusting βCD concentration under equilibrium. It is notable that the gel can recover the original elasticity value once immersed into βCD-free solution.

Figure 2a represents the influence of total concentration of monomers C_m on the optical transparency and the elastic modulus obtained by the compression test with a creep meter (E_{bulk}) at a constant fraction of host- and guest monomers ($x = 2$ mol%). As presented in the figure, the sample seemed opaque at a low monomer concentration, $C_m = 1.0\,mol\,kg^{-1}$. The increase in C_m to $2.0\,mol\,kg^{-1}$ led to a monotonic increase in the elastic modulus to $E_{bulk} = 15$ kPa, and the gel became transparent at $C_m \geq 1.5\,mol\,kg^{-1}$. Further increase in C_m did not result in any remarkable change in E_{bulk}. Previously, Horkay *et al.* reported that the saturation of E_{bulk} occurs at a volume fraction (φ) of $\varphi \approx 0.2$ in the case of poly(acrylamide)[52]. In our experimental system, $C_m > 2.0\,mol\,kg^{-1}$ corresponds to $\varphi > 0.2$. Thus, we concluded $C_m = 2.0\,mol\,kg^{-1}$ is optimal for our purpose. Figure 2b shows the influence of the molar fraction of host- and guest monomers x on E_{bulk}, while keeping C_m constant at $2.0\,mol\,kg^{-1}$. A clear increase in E_{bulk} in accord with the increase in x from 1 to 3 mol%. However, we found that the gel becomes opaque and E_{bulk} took a much lower value at a high molar fraction, $x > 3$ mol%. Based on these two experimental findings, we kept $C_m = 2.0\,mol\,kg^{-1}$ and $x = 2$ mol% in the following.

To examine if one can modulate the elasticity of host-guest gels by adding host molecules, we measured the Young's modulus of hydrogel samples by two methods: E_{bulk} was obtained from the linear regime of macroscopic stress-strain curves, and E_{AFM} was determined by AFM nano-indentation. As presented in Fig. 2c, E_{AFM} exhibited a remarkable decrease by increasing βCD concentration, following the change in chemical potential of βCD,

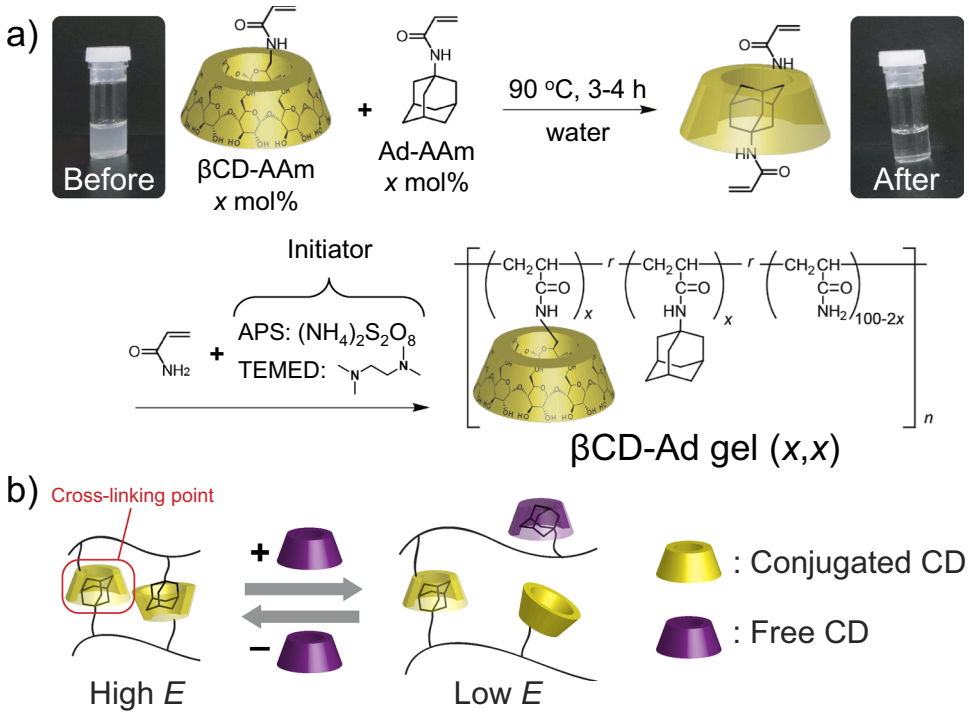

Figure 1. Working principle of host-guest gel. (**a**) Preparation and chemical structure of βCD–Ad gel (*x*,*x*). *x* represents the mol% contents of βCD and Ad units. (**b**) Reversible switching of βCD–Ad bonds in response to free βCD molecules (purple) in solution. Under equilibrium, the fraction of βCD–Ad bonds connected to the polymer chains depends on βCD concentration, which allows for the dynamic modulation of Young's modulus *E*.

$$E_{AFM} \propto \log[\beta CD] \tag{5}$$

Figure 2d represents the plot of E_{bulk} vs. E_{AFM} measured at different βCD concentrations. It should be noted that the E_{bulk} value remained stable over 24 h when a hydrogel substrate was immersed in the medium with a defined βCD concentration, confirming that E_{bulk} was measured under equilibrium. Excellent agreement between E_{bulk} and E_{AFM} implies that free βCD molecules in solution can diffuse inside the hydrogel samples, resulting in the modulation of the Young's modulus of the whole hydrogel substrates with the thickness up to 200 μm. In the next step, E_{AFM} was measured in the absence and presence of 5 mM βCD under different temperature conditions (Fig. 2e). The elastic modulus exhibited a clear decrease both in the presence and absence of free βCD in solution at elevated temperature. This finding suggests that the gels consist of three-dimensional networks of high molecular weight polymers like rubber and thus the elasticity is dominated by entropy[53]. Figure 2f represents the dynamic modulation of E_{AFM} in response to the repetitive exchange of media with and without free βCD in solutions at $T = 37$ °C. Initially, the elasticity of hydrogel substrates in the absence of free βCD in solutions ([βCD] = 0 mM) was $E_{AFM} \approx 11$ kPa, and the exposure to the medium containing 2.5 mM free βCD in the solution (●) led to an abrupt decrease in the elasticity, $E_{AFM} \approx 7$ kPa. After confirming the equilibration, the medium was exchanged to βCD-free medium, which resulted in a recovery of the elasticity to the initial level, $E_{AFM} \approx 11$ kPa. Several cycles were repeated to guarantee that the modulation of the substrate elasticity is fully reversible. The experiments with 10 mM βCD (▲) also exhibited a fully reversible modulation of E_{AFM}. As expected from the results presented in Fig. 2d, we obtained a lower $E_{AFM} \approx 4$ kPa with 10 mM βCD, demonstrating that the magnitude of switching can be adjusted by βCD concentration.

Figure 3a represents the maximum swelling ratio $[\Delta d/d_0]_{max}$ plotted as a function of βCD concentration. The acquired data can be represented empirically by a single negative exponential fit (Fig. 3a, solid line) with the characteristic concentration $[\beta CD]_c = 10.3$ mM. The addition of 10 mM βCD led to an increase in the film thickness from 72 μm to 133 μm, resulting in the swelling ratio of about 0.9. The insets show two confocal images of the gel (side views), whose surfaces were functionalized with the fluorescently labeled fibronectin. Figure 3b shows the dynamic change in the swelling ratio ($\Delta d/d_0$) as a function of time under repetitive exchanges of the βCD-free medium and the media with [βCD] = 6 mM (●), 10 mM (■), and 20 mM (▲). The swelling ratio reaches to its saturation level in about 1 h after the medium exchange in both directions. The apparent difference between the change in E_{AFM} and the change in swelling ratio can be attributed to the difference in the length scales between the AFM indentation (<1 μm) and Δd (>50 μm) as reported previously[54].

Biological cells do not only deform the substrate by generating active traction forces[55–57] but also react to the lateral strain of substrates[58,59]. Therefore, towards the dynamic regulation of cells, it is highly important to check if the swelling of hydrogels is isotropic. For this purpose, we embedded fluorescently labeled latex particles in the

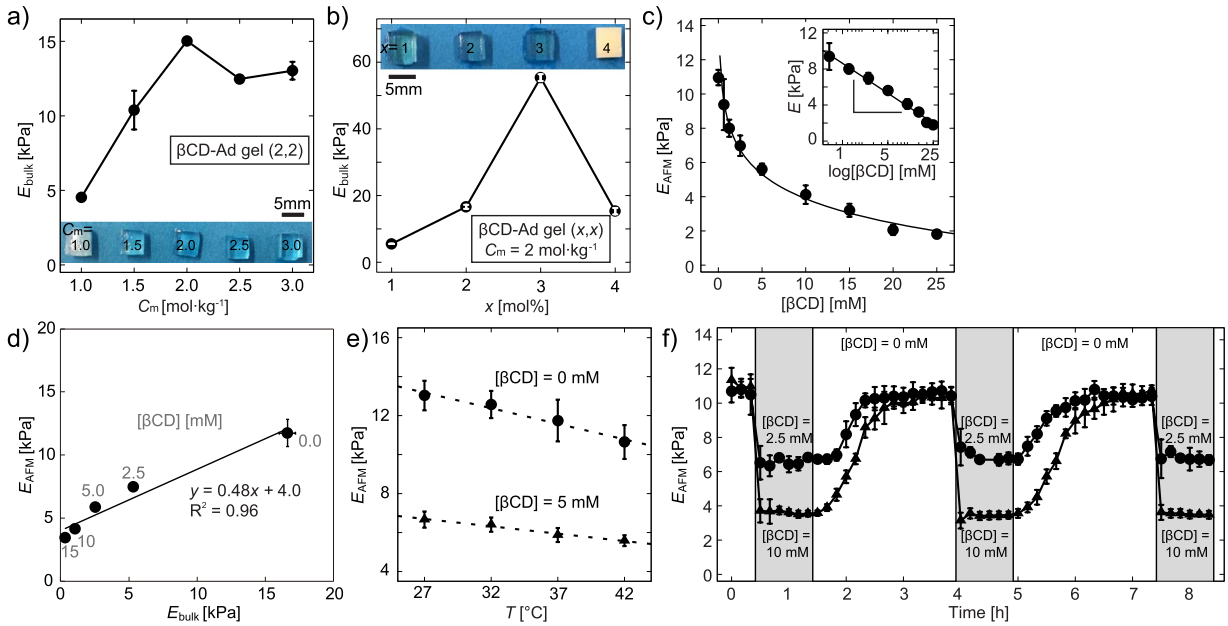

Figure 2. Macroscopic and microscopic gel assessment. (**a**) Young's modulus E_{bulk} of βCD–Ad gel (2,2) vs. total monomer concentration $C_m = 1.0$, 1.5, 2.0, 2.5, and 3.0 mol kg^{-1}, measured by a creep meter. (**b**) E_{bulk} plotted as a function of the mol% content of βCD–AAm and Ad–AAm monomers in the monomer solution (x), while keeping $C_m = 2.0$ mol·kg^{-1} constant. (**c**) E_{AFM} of βCD–Ad gel (2, 2) vs. βCD concentration, measured at RT. The change in elasticity shows a clear dependence on βCD concentration; $\Delta E_{AFM} \propto \log[\beta CD]$. (**d**) Correlation between E_{bulk} measured by a creep meter and E_{AFM} measured by AFM indentation. βCD–Ad gel (2,2) with $C_m = 2.0$ mol kg^{-1} was immersed into RPMI 1640 medium containing 0, 2.5, 5.0, 10, and 15 mM of βCD. (**e**) Temperature dependence of E_{AFM} in the presence and absence of 5 mM βCD. (**f**) *In situ* modulation of E_{AFM} at $T = 37$ °C. Reversible switching of the substrate elasticity was confirmed by alternatively changing βCD concentration in the solution between 0 and 2.5 mM (●) as well as 0 and 10 mM (▲).

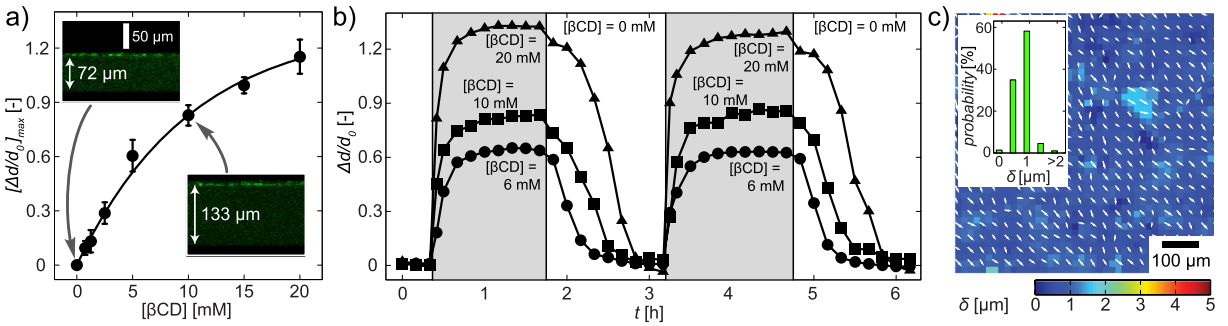

Figure 3. Reversible switching of thickness by medium exchange. (**a**) Maximum swelling ratio $[\Delta d/d_0]_{max}$ plotted as a function of βCD concentration. The insets show two representative cross-sectional images of gels at [βCD] = 0 and 10 mM, reconstructed from the confocal fluorescence microscopy images. Here, fibronectin labeled with HiLyte Fluor™ 488 was used to confirm the uniform functionalization of gel surfaces. The black line is the fit of the equation $f([\beta CD]) \propto 1 - \exp(-[\beta CD]/[\beta CD]_c)$ (6) with the characteristic concentration $[\beta CD]_c = 10.3$ mM. (**b**) Reversible switching of $\Delta d/d_0$ by repetitive exchanges of media with different βCD concentration; 6 mM (●), 10 mM (■), and 20 mM (▲). (**c**) The lateral displacement of fluorescent beads embedded in the gel caused by the incubation with 10 mM βCD for 40 min. The magnitude of displacement is indicated by the color code, while the direction is indicated by the arrows. The histogram in the inset represents the distribution of displacements, implying that the lateral displacement is ≤1 μm for more than 90% of the beads.

host-guest gel, and monitored the lateral displacement caused by swelling using confocal microscopy (Supporting Information S4). Figure 3c represents the lateral deformation of the gel analyzed by measuring the displacement of embedded fluorescent beads and using particle image velocimetry (PIV) after the incubation in the medium containing 10 mM βCD. The magnitude of displacement is indicated by the color code, while arrows indicate the direction. Although the swelling of the film is $\Delta d_{max} \approx 60$ μm, as shown in Fig. 3a, the histogram of displacement (inset) implies that the lateral displacement is ≤1 μm for more than 90% of the beads. This finding confirms that exposure to βCD induces swelling of host-guest gels in the direction normal to the substrate but does not exert

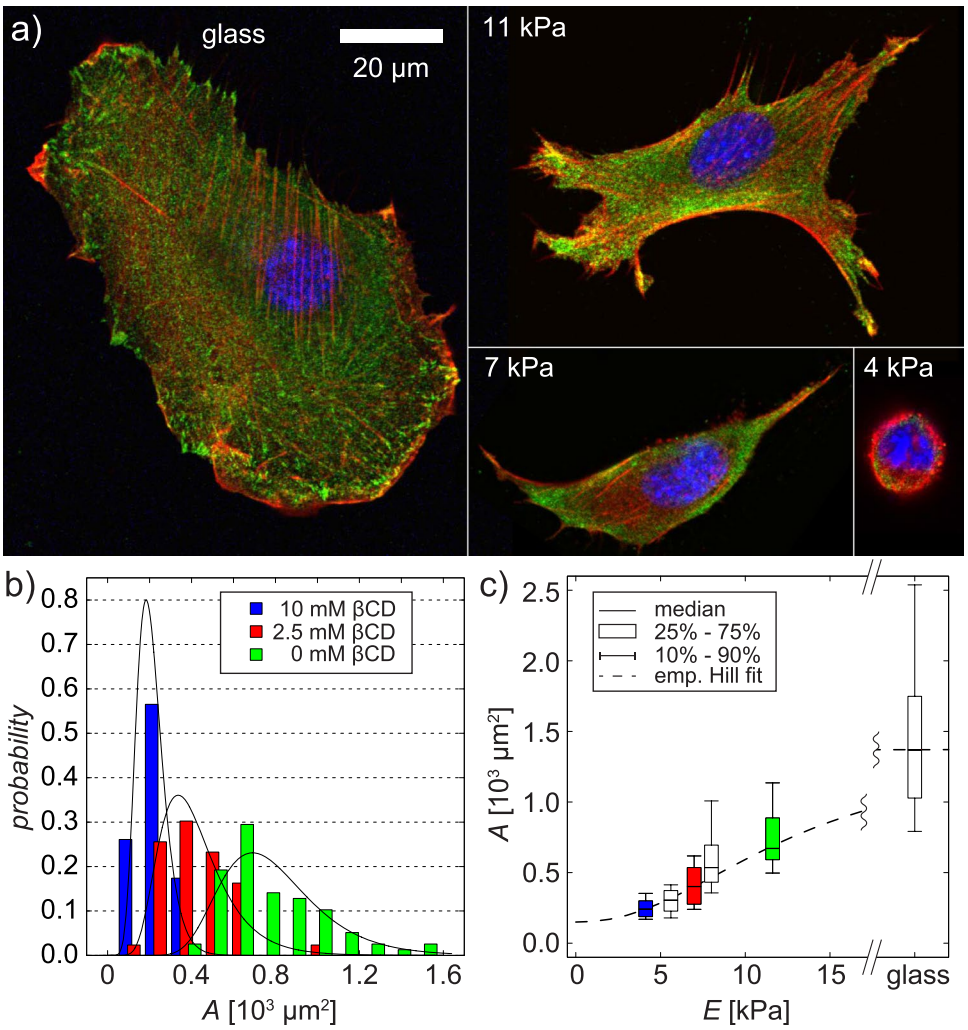

Figure 4. *Ex situ* mechano-sensing of C2C12. (**a**) Confocal fluorescence images of C2C12 cells on glass substrates ($E \approx 50$ GPa, control), and host-guest gel substrates with $E = 11$, 7, and 4 kPa. All the substrates were functionalized with fibronectin. Vinculin (green), actin (red), and nuclei (blue). (**b**) Histograms of the projected areas A of C2C12 cells at [βCD] = 0 (green), 2.5 (red), and 10 mM (blue), taken from a total number of $n > 150$ cells. The distribution for each condition could be well fitted with a log-normal function. (**c**) Projected area as a function of the elastic modulus of the gel, fitted with the empirical Hill equation (broken line).

shear force on the cells caused by lateral deformation. As reported previously[60], such an anisotropic swelling of hydrogels could be attributed to the physical constrain of the host-guest gel, whose bottom side is covalently anchored to the solid substrates.

As the first step towards the mechanical regulation of cells using host-guest gel substrates, we monitored how C2C12 cells sense the substrate elasticity *ex situ*. Here, we seeded C2C12 myoblasts on four different substrates; glass ($E \approx 50$ GPa, control) and host-guest gel substrates equilibrated with [βCD] = 0 ($E \approx 11$ kPa), 2.5 ($E \approx 7$ kPa), and 10 mM ($E \approx 4$ kPa). Figure 4a shows the representative confocal fluorescence images of C2C12 cells on four substrates, showing the overlay of vinculin (green), actin (red), and nuclei (blue). First, according to the increase in the substrate elasticity E, we found more concentrated focal adhesions and more pronounced actin stress fibers. Moreover, we found that the projected area of cells A monotonically increased according to the increase in E. The statistical reliability of the observed tendency was verified by taking the histogram from more than 23 cells for each substrate (Fig. 4b), which can be well fitted with a log-normal function. As presented in Fig. 4c, the dependence of projected area A on substrate elasticity E can be fitted by the empirical Hill equation (broken line):

$$A(E) = \frac{A_{max}}{\left(\left(\frac{E_{\frac{1}{2}}}{E}\right)^{m} + 1\right)} + A_{min}. \tag{7}$$

The median area on the glass was taken as $A_{max} = 1217\,\mu m^2$, while the median area on the softest substrate ($E \approx 4$ kPa) was set as the minimum level $A_{min} = 150\,\mu m^2$. The half level, $E_{1/2} \approx 13$ kPa, represents the characteristic

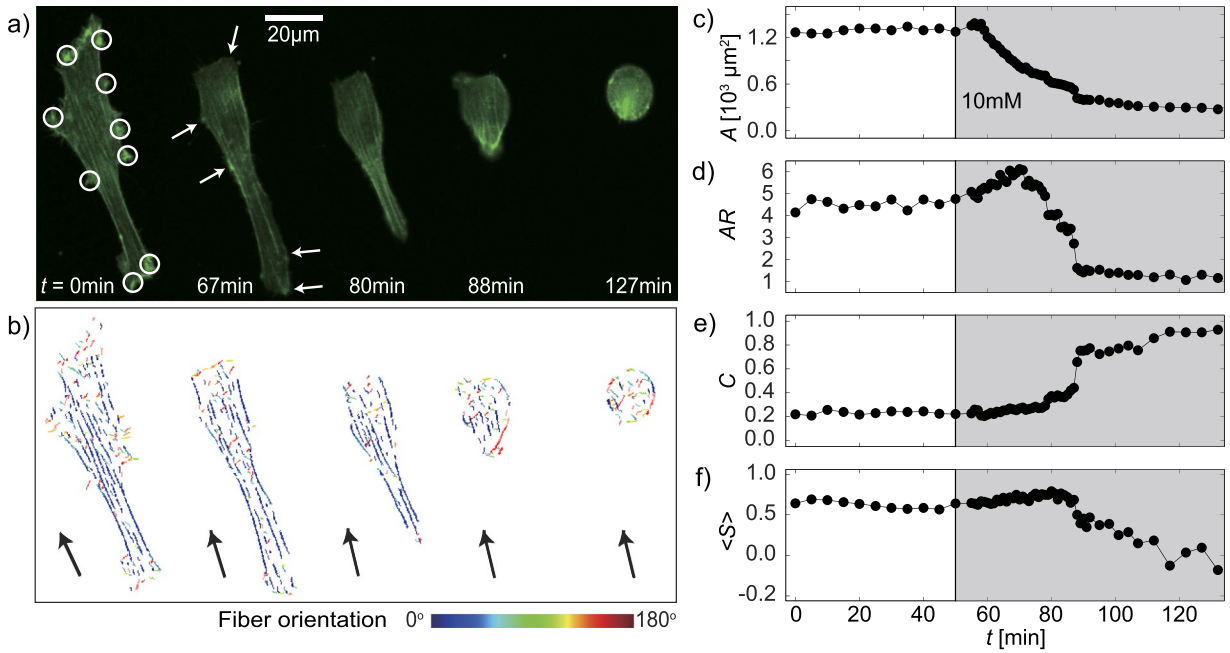

Figure 5. *In situ* mechano-response of C2C12. Dynamic response of C2C12 myoblasts upon the softening of βCD–Ad gel (2,2) from $E \approx 11$ to 4 kPa, caused by the exchange to the medium containing 10 mM of βCD. (**a**) Snapshot images of a C2C12 cell from the live cell imaging (LifeAct-GFP). (**b**) Actin cytoskeletons extracted from the images. Changes in (**c**) projected cell area A, (**d**) aspect ratio AR, (**e**) circularity C, and (**f**) nematic order parameter of actin cytoskeleton $<S>$ are plotted over time. The medium was exchanged at $t = 50$ min, and medium containing βCD was continuously supplied in the shaded time zone.

E value for the cell spreading, while $m_{=}2.2$ is the cooperativity coefficient[61]. The obtained $E_{1/2}$ value for C2C12 on host-guest gels seems to agree well with those of C2C12 on other materials reported previously, such as $E_{1/2} \approx 23$ kPa on pH sensitive gels[28] and $E_{1/2} \approx 7.6$ kPa on photo-crosslinked gelatin gels[50]. Actually, $E_{1/2} \approx 13$ kPa agrees very well with the optimal elastic modulus of $E \approx 12$ kPa for actomyosin striations[9] as well as for the stabilization of cardiac conduction[62,63]. Therefore, our host-guest gels are ideally suited to modulate the Young's modulus of the substrates between the optimal level and the softer regime for myoblasts.

In the next step, we focused on the dynamic, *in situ* response of C2C12 to the softening of the substrate elasticity from $E \approx 11$ kPa to 4 kPa by the transient transfection with LifeAct-GFP to visualize actin cytoskeletons. In Fig. 5a, several representative snapshot images selected from the live cell imaging were presented. Initially, long actin cytoskeletons form bundles (stress fibers) near the cell periphery to maintain the tension on the substrate with $E \approx 11$ kPa ("contractile" state). Upon the exchange from βCD-free medium to medium containing 10 mM of βCD at $t = 50$ min, the cell started changing its shape after some lag time ($\Delta t \approx 10$ min). As a result, the area A reached to the steady state at $t \approx 90$ min, where the cell took a round shape ("resting" state). As shown in Fig. 5b, the actin cytoskeletons became shorter and more isotropic during the transition from the "contractile" to "resting" states. To gain further insights into the dynamic response, changes in the standard morphometric parameters were plotted as a function of time; projected area A (Fig. 5c), aspect ratio AR (Fig. 5d), and circularity C (Fig. 5e). The projected area A starts monotonical decreasing after $t \approx 60$ min, which coincides with the first detachment of focal adhesions. The fact that A did not show a remarkable increase seems reasonable from the lack of lateral expansion by the addition of competitive βCD (Fig. 3c). This time lag Δt is slightly different between cells because of the stochasticity of the bond detachment under the softening of the substrates. On the other hand, the aspect ratio AR first exhibited an increase until $t \approx 70$ min, followed by an abrupt decrease. The apparent increase in AR can be attributed to the strong pinning of the focal adhesions (indicated by white circles in Fig. 5a), which remained even after the detachment of some other focal contacts (indicated by white arrows in Fig. 5a). Nevertheless, AR rapidly decreased once these contacts were detached, reaching to $AR \approx 1$ (round, resting cell). The circularity C remained almost constant at a low level ($C \approx 0.2$) until AR started dropping rapidly. This tendency seems consistent with the fact that C2C12 did not exhibit remarkable protrusions (filipodia) even at the contractile state. The identification of actin filaments from the live cell images (Fig. 5b) further allows for the calculation of nematic order parameter of actin filaments, $\langle S \rangle = \langle \cos 2\theta \rangle$ (4), where θ is defined as an azimuth angle between the actin filament and the major axis of the cell. As presented in Fig. 5f, the nematic order parameter $<S>$ showed a high level ($<S> \approx 0.6$) at $E \approx 11$ kPa, which agrees well with the previous account that reported the optimal striation of actomyosin complexes at $E \approx 12$ kPa[9]. As shown in Fig. 5f, $<S>$ started decreasing at a much later time point than the shape adaptation as previously reported[64]. In fact, the actin filaments first got shorter before changing their orientation from nematic to isotropic, corresponding the distinct delay before $<S>$ started decaying. This finding seems to agree well with the previous accounts, reporting the more pronounced alignment of actin fibers along the major axis according to the increase in substrate elasticity, because

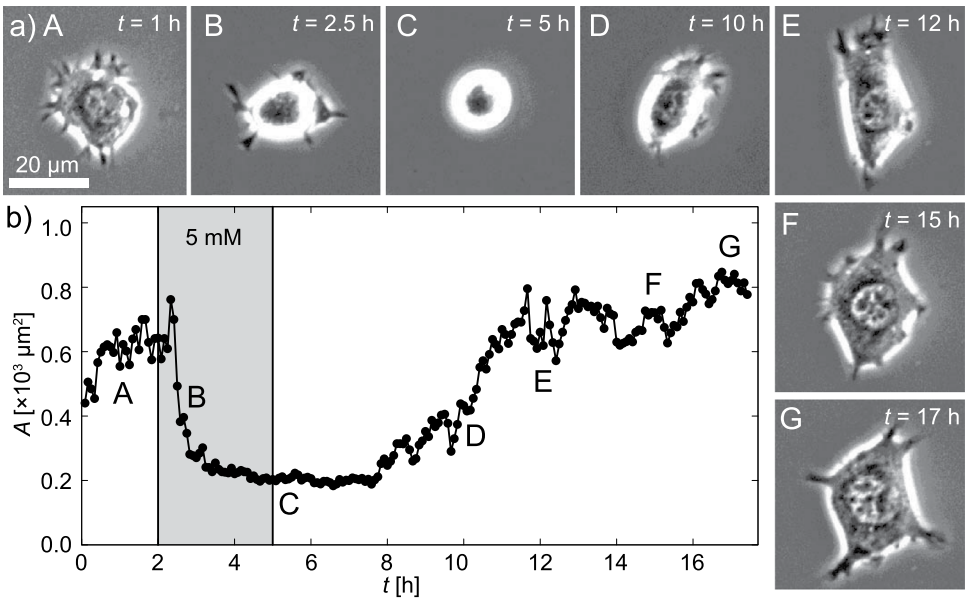

Figure 6. Reversible switching of cell morphology by mechanical commands. (**a**) Some representative phase contrast images are presented in subpanels A – G. C2C12 cells were exposed to medium containing 5 mM of βCD from $t = 2$ to 5 h (shaded time zone). (**b**) Projected area A of C2C12 plotted over time. The response of C2C12 to the substrate "softening" from $E \approx 11$ to 6 kPa occurred much faster than the reverse reaction. The lag time before the cell started responding was also found to be much shorter for the softening. (See Supporting Information Fig. S2 for other examples.)

the alignment of actin cytoskeletons and the formation of stress fibers are regulated by the force transmission via actomyosin complexes[30,49,65].

However, in contrast to our previous study using pH responsive gels functionalized with physisorbed fibronectin[29], we observed no discontinuous change in the order parameter (referred to the break of symmetry) during the mechano-response of C2C12. The different observations might be explained potentially by the following several reasons. First, the characteristic time for the elasticity change caused by the competitive host-guest interaction in this system is much longer than that of hydrogels that change the elasticity by pH change, following a clear difference in the diffusibility of βCD vs. H^+. In case of "softening", the change in Young's modulus completed after 10–30 min (Fig. 2f). This partially overlaps with the time window of cellular response (the lag time $\Delta t \approx 10$ min, the time to reach the equilibrium ≈ 40 min). This might cause a more progressive change in the cytoskeletal ordering. Another scenario is the magnitude of the change in substrate elasticity. In our previous system, the substrate elasticity was modulated from 40 kPa to 2 kPa, which covers a critical substrate elasticity proposed recently by Yip *et al.*; 20 kPa[66]. In this account, it has been suggested that mouse embryonic fibroblast remodels the actin cytoskeletons and retains the substrate strain at a constant level when the Young's modulus of the substrate was below 20 kPa. On the other hand, they observed the conservation of stress when the Young's modulus was above 20 kPa, which agrees well with the theoretical prediction[49,67]. Although these studies dealt with different cells (fibroblast and mesencymal stem cells), it is plausible that the critical substrate elasticity at which C2C12 myoblast switches the mechano-response may exist around this level. Actually, the conduction of cardiomyocyte tissues was significantly promoted near 13 kPa[62]. Further studies with substrates with higher elastic modulus (e.g. ≈50 kPa, Fig. 2b) would enable us to determine the critical elasticity jump that causes the symmetry break of the nematic order parameter of actin filaments.

Figure 6a represents a series of phase contrast images of C2C12 that underwent the reversible switching of its morphology under a medium exchange cycle. Initially, cells were seeded in βCD-free medium. At $t = 2$ h the medium was exchanged to the one containing 5 mM of βCD, and the cell was kept under this condition for 3 h. After confirming the equilibration of the system, the medium was exchanged back to the original βCD-free medium. The projected area A of C2C12 was plotted as a function of time in Fig. 6b. The exchange from βCD-free to βCD-containing medium (corresponding to E from 11 kPa to 6 kPa) led to a monotonic decrease in A after a short lag time ($\Delta t = 10$–20 min), which is comparable to that presented in Fig. 5. The saturation level of projected area ($A \approx 200\ \mu m^2$) seems to agree well with the one obtained from the *ex situ* experiments, $A_{ex\ situ} = 240 \pm 60\ \mu m^2$ (Fig. 4c), confirming that the system reached to equilibrium. At $t = 5$ h, the medium was exchanged back to βCD-free medium. Compared to the "softening" of the host-guest gel substrate, the cellular response to the substrate "stiffening" was found to be much slower. As presented in the figure, the lag time before the visible response was almost 3 h. Such an extremely long lag time here could be explained by the combination of two factors. First, as presented in Figs 2f and 3b, the characteristic time required for the stiffening of host-guest gels is about 1–1.5 h, which is in contrast to the softening that is completed after 10–30 min. Moreover, it is plausible that the spreading of cells requires more time than the contraction. The spreading of cells requires both the establishment of focal contacts and the propagation of spreading fronts. In contrast, the contraction is dominated by cortical tension

and the kinetics of actin depolymerization once the focal contacts are cancelled. In fact, the treatment of C2C12 on a stiff substrate (40 kPa) resulted in a fast contraction, while leaving the focal contacts behind[64]. Nevertheless, the projected area A increased to 600–800 μm^2, which is comparable to the initial level ($A \approx 600\,\mu m^2$ at $t = 2$ h) and the *ex situ*, equilibrium level, $A_{ex\ situ} = 620 \pm 80\,\mu m^2$ (Fig. 4c). Previously, βCD has been used to deplete the cholesterol and influence the integrin clustering in heat-shocked, Drosophila cells[68]. In this study, we performed control experiments on fibronectin-coated glass substrates (Fig. S2) and polyacrylamide containing no host-guest side chains (Fig. S4), verifying that the presence of βCD does not cause major change in cell shape, adhesion area and cytoskeletal order parameter. Recent studies evidenced that not only the substrate elasticity but also the viscosity influences the dynamic cellular response, such as cell spreading and proliferation[69,70]. The combination with rheological study would enable the optimization of the time windows to investigate the interplay of elasticity and viscosity of substrates.

Conclusions

In this study, we utilized a new class of hydrogel materials, cross-linked by host-guest interactions, and demonstrated the potential for the dynamic regulation of cell-substrate interactions. Taking the advantage of reversible, supramolecular cross-linkers based on βCD and adamantane, the substrate elasticity can be modulated by exchanging the culture medium with and without free host molecules (βCD). As the modulation of magnitude and direction of the substrate elasticity can be achieved by varying the concentrations of free βCD in solutions, such "host-guest gels" enable one to apply dynamic mechanical stresses to cells by altering the substrate elasticity at a desired time point. In this study, we fabricated a host-guest gel, whose elastic modulus can be adjusted between 4 and 11 kPa. In the first step, we systematically investigated the influence of monomer ratios between host, guest, and matrix monomers on the substrate elasticity. Second, we demonstrated that the elasticity of host-guest gels depends on free βCD concentrations. The projected area of C2C12 on substrates exhibited a clear correlation with the substrate elasticity, and the fitting of the experimental results with the empirical Hill equation indicated that the elasticity of our host-guest gel covers the optimal range for regulating myoblasts. Such *ex situ* experiments under static conditions were further extended to monitor the dynamic, *in situ* response of cells to the change in substrate elasticity. In addition to the commonly used morphological parameters such as aspect ratio and circularity, we tracked the dynamic remodeling of cytoskeletons by calculating the nematic order parameter $<S>$ of actin cytoskeletons from live cell images. The softening of substrates led to the detachment of focal adhesion contacts, followed by the morphological change from a stretched, contractile shape to a round shape, reflecting the depolymerization and disordering of actin cytoskeletons. Furthermore, we confirmed such a dynamic mechano-response of C2C12 is fully reversible under softening and stiffening of the gel substrate. Supramolecular hydrogels based on host-guest cross-linkers provide with a major advantage over recently reported materials that can either change the substrate elasticity only in a unidirectional manner or utilize more stressful cues for cells, such as temperature and UV light. Therefore, our host-guest gels open a new avenue not only for understanding the fundamental mechanism of dynamic cellular response to matrix remodeling, but also for a potential to mechanically direct the cell fate in *in vitro* culture.

References

1. Vogel, V. & Sheetz, M. Local force and geometry sensing regulate cell functions. *Nat. Rev. Mol. Cell Biol.* **7**, 265–275 (2006).
2. Discher, D. E., Janmey, P. & Wang, Y.-l Tissue Cells Feel and Respond to the Stiffness of Their Substrate. *Science* **310**, 1139–1143 (2005).
3. Harburger, D. S. & Calderwood, D. A. Integrin signalling at a glance. *J. Cell Sci.* **122**, 1472–1472 (2009).
4. Vinogradova, O. *et al*. A Structural Mechanism of Integrin αIIbβ3 "Inside-Out" Activation as Regulated by Its Cytoplasmic Face. *Cell* **110**, 587–597 (2002).
5. Rosales, A. M. & Anseth, K. S. The design of reversible hydrogels to capture extracellular matrix dynamics. *Nat. Rev. Mater.* **1**, 15012 (2016).
6. Kidoaki, S. & Matsuda, T. Microelastic gradient gelatinous gels to induce cellular mechanotaxis. *J. Biotechnol.* **133**, 225–230 (2008).
7. Wen, J. H. *et al*. Interplay of matrix stiffness and protein tethering in stem cell differentiation. *Nat. Mater.* **13**, 979–987 (2014).
8. Engler, A. *et al*. Substrate Compliance versus Ligand Density in Cell on Gel Responses. *Biophys. J.* **86**, 617–628 (2004).
9. Engler, A. J. *et al*. Myotubes differentiate optimally on substrates with tissue-like stiffness: pathological implications for soft or stiff microenvironments. *J. Cell Biol.* **166**, 877–887 (2004).
10. Ghajar, C. M. *et al*. The Effect of Matrix Density on the Regulation of 3-D Capillary Morphogenesis. *Biophys. J.* **94**, 1930–1941 (2008).
11. Lo, C.-M., Wang, H.-B. & Dembo, M. & Wang, Y.-l. Cell Movement Is Guided by the Rigidity of the Substrate. *Biophys. J.* **79**, 144–152 (2000).
12. Kawano, T. & Kidoaki, S. Elasticity boundary conditions required for cell mechanotaxis on microelastically-patterned gels. *Biomaterials* **32**, 2725–2733 (2011).
13. Engler, A. J., Sen, S., Sweeney, H. L. & Discher, D. E. Matrix Elasticity Directs Stem Cell Lineage Specification. *Cell* **126**, 677–689 (2006).
14. Discher, D. E., Mooney, D. J. & Zandstra, P. W. Growth Factors, Matrices, and Forces Combine and Control Stem Cells. *Science* **324**, 1673–1677 (2009).
15. Simmons, C. A., Alsberg, E., Hsiong, S., Kim, W. J. & Mooney, D. J. Dual growth factor delivery and controlled scaffold degradation enhance *in vivo* bone formation by transplanted bone marrow stromal cells. *Bone* **35**, 562–569 (2004).
16. Kanazawa, H. *et al*. Bone Marrow-Derived Mesenchymal Stem Cells Ameliorate Hepatic Ischemia Reperfusion Injury in a Rat Model. *Plos One* **6** (2011).
17. Wolf, K. *et al*. Compensation mechanism in tumor cell migration: mesenchymal–amoeboid transition after blocking of pericellular proteolysis. *J. Cell Biol.* **160**, 267–277 (2003).
18. Guvendiren, M. & Burdick, J. A. Stiffening hydrogels to probe short- and long-term cellular responses to dynamic mechanics. *Nat. Commun.* **3**, 792 (2012).
19. Urban, M. W. Handbook of stimuli-responsive materials (Wiley-VCH, 2011).
20. Minko, S. Responsive polymer materials: design and applications. 1st edn (Blackwell Pub., 2006).
21. Stuart, M. A. C. *et al*. Emerging applications of stimuli-responsive polymer materials. *Nat. Mater.* **9**, 101–113 (2010).

22. Yan, X., Wang, F., Zheng, B. & Huang, F. Stimuli-responsive supramolecular polymeric materials. *Chem. Soc. Rev.* **41**, 6042–6065 (2012).
23. Yang, C., Tibbitt, M. W., Basta, L. & Anseth, K. S. Mechanical memory and dosing influence stem cell fate. *Nat. Mater.* **13**, 645–652 (2014).
24. Okano, T., Yamada, N., Okuhara, M., Sakai, H. & Sakurai, Y. Mechanism of cell detachment from temperature-modulated, hydrophilic-hydrophobic polymer surfaces. *Biomaterials* **16**, 297–303 (1995).
25. Nishida, K. *et al.* Corneal Reconstruction with Tissue-Engineered Cell Sheets Composed of Autologous Oral Mucosal Epithelium. *New Eng. J. Med.* **351**, 1187–1196 (2004).
26. Shu, X. Z., Liu, Y., Luo, Y., Roberts, M. C. & Prestwich, G. D. Disulfide Cross-Linked Hyaluronan Hydrogels. *Biomacromolecules* **3**, 1304–1311 (2002).
27. Shu, X. Z., Ahmad, S., Liu, Y. & Prestwich, G. D. Synthesis and evaluation of injectable, *in situ* crosslinkable synthetic extracellular matrices for tissue engineering. *J. Biomed. Mater. Res. A* **79A**, 902–912 (2006).
28. Yoshikawa, H. Y. *et al.* Quantitative Evaluation of Mechanosensing of Cells on Dynamically Tunable Hydrogels. *J. Am. Chem. Soc.* **133**, 1367–1374 (2011).
29. Inoue, S. *et al.* Live cell tracking of symmetry break in actin cytoskeleton triggered by abrupt changes in micromechanical environments. *Biomater. Sci.* **3**, 1539–1544 (2015).
30. Frank, V. *et al.* Frequent mechanical stress suppresses proliferation of mesenchymal stem cells from human bone marrow without loss of multipotency. *Sci. Rep.* **6**, 24264 (2016).
31. Kakuta, T. *et al.* Preorganized Hydrogel: Self-Healing Properties of Supramolecular Hydrogels Formed by Polymerization of Host–Guest-Monomers that Contain Cyclodextrins and Hydrophobic Guest Groups. *Adv. Mater.* **25**, 2849–2853 (2013).
32. Nakahata, M., Takashima, Y. & Harada, A. Highly Flexible, Tough, and Self-Healing Supramolecular Polymeric Materials Using Host–Guest Interaction. *Macromol. Rapid Commun.* **37**, 86–92 (2016).
33. Rodell, C. B., Kaminski, A. L. & Burdick, J. A. Rational Design of Network Properties in Guest–Host Assembled and Shear-Thinning Hyaluronic Acid Hydrogels. *Biomacromolecules* **14**, 4125–4134 (2013).
34. Shih, H. & Lin, C.-C. Tuning stiffness of cell-laden hydrogel via host-guest interactions. *J. Mater. Chem. B* **4**, 4969–4974 (2016).
35. Takashima, Y. *et al.* Expansion–contraction of photoresponsive artificial muscle regulated by host–guest interactions. *Nat. Commun.* **3**, 1270 (2012).
36. Nakahata, M., Takashima, Y., Yamaguchi, H. & Harada, A. Redox-responsive self-healing materials formed from host–guest polymers. *Nat. Commun.* **2**, 511 (2011).
37. Stella, V. J. & He, Q. Cyclodextrins. *Toxicol. Pathol.* **36**, 30–42 (2008).
38. Katarina, S. *et al.* Adamantane – A Lead Structure for Drugs in Clinical Practice. *Curr. Med. Chem.* **23**, 3245–3266 (2016).
39. Kern, W. & Puotinen, D. A. Cleaning solutions based on hydrogen peroxide for use in silicon semiconductor technology. *RCA Rev.* **31**, 187–206 (1970).
40. Harada, A., Kobayashi, R., Takashima, Y., Hashidzume, A. & Yamaguchi, H. Macroscopic self-assembly through molecular recognition. *Nat. Chem.* **3**, 34–37 (2011).
41. Tse, J. R. & Engler, A. J. In *Current Protocols in Cell Biology* (John Wiley & Sons, Inc., 2001).
42. Aratyn-Schaus, Y., Oakes, P. W., Stricker, J., Winter, S. P. & Gardel, M. L. Preparation of Complaint Matrices for Quantifying Cellular Contraction. *J. Vis. Exp.: JoVE*, 2173 (2010).
43. Milner, S. T., Witten, T. A. & Cates, M. E. Theory of the grafted polymer brush. *Macromolecules* **21**, 2610–2619 (1988).
44. Kuhl, T. L. *et al.* A Neutron Reflectivity Study of Polymer-Modified Phospholipid Monolayers at the Solid-Solution Interface: Polyethylene Glycol-Lipids on Silane-Modified Substrates. *Biophys. J.* **75**, 2352–2362 (1998).
45. Rossetti, F. F., Schneck, E., Fragneto, G., Konovalov, O. V. & Tanaka, M. Generic Role of Polymer Supports in the Fine Adjustment of Interfacial Interactions between Solid Substrates and Model Cell Membranes. *Langmuir* **31**, 4473–4480 (2015).
46. Domke, J. & Radmacher, M. Measuring the Elastic Properties of Thin Polymer Films with the Atomic Force Microscope. *Langmuir* **14**, 3320–3325 (1998).
47. Rotsch, C., Jacobson, K. & Radmacher, M. Dimensional and mechanical dynamics of active and stable edges in motile fibroblasts investigated by using atomic force microscopy. *Proc. Natl. Acad. Sci.* **96**, 921–926 (1999).
48. Lin, D. C., Dimitriadis, E. K. & Horkay, F. Robust Strategies for Automated AFM Force Curve Analysis—I. Non-adhesive Indentation of Soft, Inhomogeneous Materials. *J. Biomech. Eng.* **129**, 430–440 (2006).
49. Zemel, A., Rehfeldt, F., Brown, A. E. X., Discher, D. E. & Safran, S. A. Optimal matrix rigidity for stress fiber polarization in stem cells. *Nat. Phys.* **6**, 468–473 (2010).
50. Yoshikawa, H. Y., Kawano, T., Matsuda, T., Kidoaki, S. & Tanaka, M. Morphology and Adhesion Strength of Myoblast Cells on Photocurable Gelatin under Native and Non-native Micromechanical Environments. *J. Phys. Chem. B* **117**, 4081–4088 (2013).
51. Otsu, N. A Threshold Selection Method from Gray-Level Histograms. *IEEE Trans. Syst., Man, Cybern., Syst.* **9**, 62–66 (1979).
52. Horkay, F., Basser, P. J., Hecht, A.-M. & Geissler, E. Structural investigations of a neutralized polyelectrolyte gel and an associating neutral hydrogel. *Polymer* **46**, 4242–4247 (2005).
53. Nishinari, K., Koide, S. & Ogino, K. On the temperature dependence of elasticity of thermo-reversible gels. *J. Phys. France* **46**, 793–797 (1985).
54. Shibayama, M., Uesaka, M. & Shiwa, Y. Swelling/shrinking kinetics of chemically cross-linked poly(vinyl alcohol) gels in the presence of borate ions. *J. Chem. Phys.* **105**, 4350–4357 (1996).
55. Harris, A., Wild, P. & Stopak, D. Silicone rubber substrata: a new wrinkle in the study of cell locomotion. *Science* **208**, 177–179 (1980).
56. Oliver, T., Dembo, M. & Jacobson, K. Separation of Propulsive and Adhesive Traction Stresses in Locomoting Keratocytes. *J. Cell Biol.* **145**, 589–604 (1999).
57. Balaban, N. Q. *et al.* Force and focal adhesion assembly: a close relationship studied using elastic micropatterned substrates. *Nat. Cell Biol.* **3**, 466–472 (2001).
58. Naruse, K. & Sokabe, M. Involvement of stretch-activated ion channels in Ca2+ mobilization to mechanical stretch in endothelial cells. *Am. J. Physiol. Cell Physiol.* **264**, C1037–C1044 (1993).
59. Akhyari, P. *et al.* Mechanical Stretch Regimen Enhances the Formation of Bioengineered Autologous Cardiac Muscle Grafts. *Circulation* **106**, I-137-I-142 (2002).
60. Suzuki, A. & Hara, T. Kinetics of one-dimensional swelling and shrinking of polymer gels under mechanical constraint. *J. Chem. Phys.* **114**, 5012–5015 (2001).
61. Ferrell, J. E. Building a cellular switch: more lessons from a good egg. *BioEssays* **21**, 866–870 (1999).
62. Hörning, M., Kidoaki, S., Kawano, T. & Yoshikawa, K. Rigidity Matching between Cells and the Extracellular Matrix Leads to the Stabilization of Cardiac Conduction. *Biophys. J.* **102**, 379–387 (2012).
63. Hörning, M. & Entcheva, E. In *Bottom-Up Self-Organization in Supramolecular Soft Matter: Principles and Prototypical Examples of Recent Advances* (eds Stefan C. Müller & Jürgen Parisi) 237–258 (Springer International Publishing, 2015).
64. Burk, A. S. *et al.* Quantifying Adhesion Mechanisms and Dynamics of Human Hematopoietic Stem and Progenitor Cells. *Sci. Rep.* **5**, 9370 (2015).
65. Trichet, L. *et al.* Evidence of a large-scale mechanosensing mechanism for cellular adaptation to substrate stiffness. *Proc. Natl. Acad. Sci.* **109**, 6933–6938 (2012).

66. Yip, A. K. *et al*. Cellular Response to Substrate Rigidity Is Governed by Either Stress or Strain. *Biophys. J.* **104**, 19–29 (2013).
67. Marcq, P., Yoshinaga, N. & Prost, J. Rigidity Sensing Explained by Active Matter Theory. *Biophys. J.* **101**, L33–L35 (2011).
68. Dibya, D., Arora, N. & Smith, E. A. Noninvasive measurements of integrin microclustering under altered membrane cholesterol levels. *Biophys. J.* **99**, 853–861 (2010).
69. Chaudhuri, O. *et al*. Substrate stress relaxation regulates cell spreading. *Nat. Commun*. **6** (2015).
70. Chaudhuri, O. *et al*. Hydrogels with tunable stress relaxation regulate stem cell fate and activity. *Nat. Mater.* **15**, 326–334 (2015).

Acknowledgements

This work was supported by MEXT (No. 26103521 to M.T.), JSPS (No. 26247070 to M.T., 26800223 and 16K05515 to A.Y., 16809998 and 16K14065 to M.N.), EU FP7 (ActiveSoft to M.T.), German Science Foundation (SFB873 to M.T.). We are thankful to the German-Japanese HeKKSaGOn Alliance for support. M.T. thanks T. Ichikawa, N. Kioka and M. Kengaku for insightful comments on the mechano-sensing of biological cells. P.L. thanks the HeKKSaGOn Program for the fellowship. M.T. is an investigator of German Cluster of Excellence "Cell Network". WPI iCeMS supported by World Premier International Research Center Initiative (WPI), MEXT (Japan).

Author Contributions

M.T. and A.H. designed and directed the research. M.N. performed material synthesis and characterization, and M.H., P.L., and A.Y. performed biophysical experiments. M.V., S.K., and Y.T. contributed to the interpretation of results and reviewed the manuscript. M.H., M.N., P.L., and M.T. wrote the paper.

Additional Information

Supplementary information accompanies this paper at doi:10.1038/s41598-017-07934-x

Competing Interests: The authors declare that they have no competing interests.

Publisher's note: Springer Nature remains neutral with regard to jurisdictional claims in published maps and institutional affiliations.